Hydromagnetic nanofluid flow with Lorentz force, viscous dissipation, Dufour effect, first-order chemical reaction and unsteadiness

Kafunda Tuesday ⬥ ✉1, Mukonda Danny ⬥1 and Mwamba Nictor ⬥2

1Department of Mathematics and Statistics, Mulungushi University, Kabwe, Zambia.
2Department of Applied Sciences and Engineering, Eden University, Zambia.

Abstract. The objective of the study was to investigate hydromagnetic nanofluid flow with Lorentz force, viscous dissipation, Dufour effects, first order chemical reaction and unsteadiness and considering the flow between parallel plates by formulating necessary mathematical model. The study considers the dynamic viscosity and thermal conductivity of the fluid as temperature-dependent variables. The fluid is assumed to be incompressible in terms of density, and the influence of gravitational effects is deemed negligible. The governing equations for the non-Newtonian nanofluid flow, including the continuity, Navier-Stokes, energy, magnetic induction, and concentration equations, have been formulated and transformed into their non-dimensional form. Finite difference numerical approximation method has been used to approximate the systems of the governing equations in different forms. The profiles of the flow variables have been presented and analyzed. The results indicate that an increase in the thermophoresis parameter enhances the species concentration, whereas higher Schmidt numbers and chemical reaction parameters lead to a reduction in concentration profiles. Additionally, magnetic induction profiles increase with a higher Reynolds number but decrease with an increasing magnetic Prandtl number. Temperature and velocity profiles increase with an increase in Reynolds number. The study is essential in the improvements of both heat and mass transfers.

Keywords: Hydromagnetic; Nanofluid; Viscous Dissipation; Dufour; Chemical Reaction; Lorentz Force.

2020 Mathematics Subject Classification: 81-XX, 33Cxx, 11-XX. MSC2020

1 Introduction

Studies on fluid flows between parallel plates have attracted the attention of many researchers. [1] investigated the steady flow of an electrically conducting, viscous, incompressible fluid bounded by two parallel infinite insulated horizontal plates and the heat transfer through it. The upper plate was given a constant velocity while the lower plate was kept stationary. The

✉Corresponding author. Email: kaftuz25@gmail.com

viscosity of the fluid was assumed to vary with temperature. The effect of an external uniform magnetic field as well as the action of an inflow perpendicular to the plates together with the influence of the pressure gradient on the flow and temperature distributions were presented and discussed. A numerical solution for the governing non-linear ordinary differential equations was developed.

Analysis of the problem of unsteady squeezing flow of a non-Newtonian nanofluid through a porous medium between two parallel plates was conducted [5]. The effects of Hall currents and heat source were taken into consideration. The governing partial differential equations are transformed into a set of nonlinear ordinary differential equations by using similarity transformations. A homotopy perturbation method is performed to obtain analytical solutions for that system of equations. The behaviors of the tangential velocity, normal velocity, temperature, and nanoparticle concentration distributions were discussed analytically and graphically under the effect of different entering parameters.

Nanofluids have attained a big consideration from scientists because of their enriched heat transfer properties. Thickness plays a vigorous part in the effectiveness of nanofluids in the convection progressions as well. [8] planned the rheological performance of a graphene nanofluid via rotating rheometer. [16] also examined the rheological possessions of 6 carbon-based nanofluids. Currently, nanofluids are categorized as hybrid nanofluids in various modules [12]. Hybrid nanofluids become by combining two distinct nanoparticles in base fluid. The key motivation of it is to moreover advance the thermal features of nanofluids. A study on adjustable heat transmission of hybrid nanofluid under the influence of outer magnetic field was carried out. This study dealt with the CFD simulation of natural convection heat transfer of a hybrid nanofluid in an inverted T-shaped cavity partitioned and saturated by two different types of porous media [9]. Suspensions of organic and inorganic nanoparticles, i.e., MWCNTs and Fe_3O_4, in water, were selected as the working fluid. The macroscopic conservation equations for the flow field and heat transfer were modeled via volume averaging the microscopic equations inside porous media over a representative elementary volume. The effects of many parameters were investigated. The results showed that, with an increase in the Rayleigh number, porosity ratio and Darcy number ratio and decrease in the thermal conductivity ratio, the averaged Nusselt number increased.

Investigation of the innovative heat transfer in non-Newtonian hybrid nanofluid collected with entropy group was conducted. The study investigated the effects of concentration and radius ratio on convective heat transfer and entropy generation of a non-Newtonian hybrid nanofluid flowing through a concentric annulus [15]. The nanofluid was prepared by suspending tetramethylammonium hydroxide (TMAH) coated Fe_3O_4 (magnetite) nanoparticles and gum arabic (GA) coated carbon nanotubes (CNTs) in water. Variable thermal conductivity and viscosity are used in simulations. [2] examined the impact of unsteady viscous flow in a squeezing channel. Silver-gold hybrid nanofluid particles with different shapes were inserted in the base fluid engine oil. Flow and heat transfer mechanism were detected in the presence of magneto-hydrodynamics between the two parallel infinite plates. The thermal conductivity models, that is, Yamada-Ota and Hamilton-Crosser models were used to investigate various shapes (Blade, platelet, cylinder, and brick) of hybrid nanoparticles. The model was made up of paired high nonlinear partial differential equations that were then transformed into ordinary differential equations which are coupled and strong nonlinear using the boundary layer approximation.

Additionally, the analysis showed that the Yamada-Ota model of the Hybrid nanofluid gains

high temperature and velocity profile than the Hamilton-Crosser model of the hybrid nanofluid. Also, both the models showed increasing trends toward increasing the volume fraction rate of silver-gold hybrid nanoparticles. It was also observed that the hybrid nanoparticles' performance was far better than the common nanofluids. [14] investigated the flow and heat transfer of magneto-hydrodynamic squeezing nanofluid flow between two infinite parallel plates had been investigated. The fluid used was an equal mixture of Ethylene-glycol and water. This paper discusses hybrid nanoparticles, including Fe_3O_4 and MoS_2. The nonlinear equations have been solved by Akbari-Ganji's method. The effect of Harman number, base fluid, squeeze number, and Heat source on flow and heat transfer have been computed. The result shows that the Akbari-Ganji's method and the numerical method were in good agreement. Akbari-Ganji's method can be useful for such problems, and we can see that the maximum difference in velocity profile and thermal profile between AGM and the numerical method was less than one per cent.

The findings showed that velocity profile reduced by an increase in squeeze number and Hartman number. The thermal profile raised with an increase in squeeze number, but it decreased with increasing in Hartman number and heat source parameter. [4] studied the impacts of viscous dissipation, thermal radiation and Joule heating on squeezing flow current and the heat transfer mechanisms for a magneto-hydrodynamic (MHD) nanofluid flow in parallel disks during a suction/blowing process. First, the governing momentum and energy equations were transformed into a non-dimensional form and then the obtained equations were solved by the modified Adomian decomposition method (ADM), known as Duan-Rach approach (DRA).

In addition, the effects of the radiation parameter, suction/blowing parameter, magnetic parameter, squeezing number and nanoparticles concentration on the heat transfer and flow field were investigated in the results. The results showed that the fluid velocity increased with increasing suction parameter, while the temperature profile decreases with increasing suction parameter. [13] natural convection of non-Newtonian bio-nanofluids flow between two vertical flat plates was investigated numerically. Sodium Alginate (SA) and Sodium Carboxymethyl Cellulose (SCMC) are considered as the base non-Newtonian fluid, and nanoparticles such as Titania (TiO_2 and Alumina (Al_2O_3 were added to them.

The effective thermal conductivity and viscosity of nanofluids were calculated through Maxwell-Garnetts (MG) and Brinkman models, respectively. A fourth-order Runge-Kutta numerical method (NUM) and three Weighted Residual Methods (WRMs), Collocation (CM), Galerkin (GM) and Least-Square Method (LSM) and Finite-Element Method (FEM), were used to solve the present problem. The influence of some physical parameters such as nanofluid volume friction on non-dimensional velocity and temperature profiles were discussed. The results show that SCMC- TiO_2 had higher velocity and temperature values than other nanofluid structures.

2   Mathematical formulation

Figure 1 shows the physical configuration of the non-Newtonian nanofluid flow between two parallel horizontal plates in three dimensions. By the no-slip boundary condition, at time $t \leq 0$, for $0 \leq (y,z) \leq h$, the nanofluid flow variables $v(y,z,0) = 0$, $w(y,z,0) = 0$, $T(y,z,0) = T_{sp}$, $C = C_{sp}$, $H_y(y,z,0) = 0$ and $H_z(y,z,0) = 0$. When the nanofluid gets in contact with the moving plate at anytime $t > 0$, the flow variables $v(0,0,t) = V_\infty$, $w(0,0,t) = V_\infty$, $T(0,0,t) = T_{mp}$, $C(0,0,t) = C_{mp}$, $H_y(0,0,t) = H_m$ and $H_z(0,0,t) = H_m$ for $(y,z) = 0$.

When $(y, z) = h$, the flow variables $v(y, z, t) = 0$, $w(y, z, t) = 0$, $T(y, z, t) = T_{sp}$, $C(y, z, t) = C_{sp}$, $H_y(y, z, t) = 0$ and $H_z(y, z, t) = 0$.
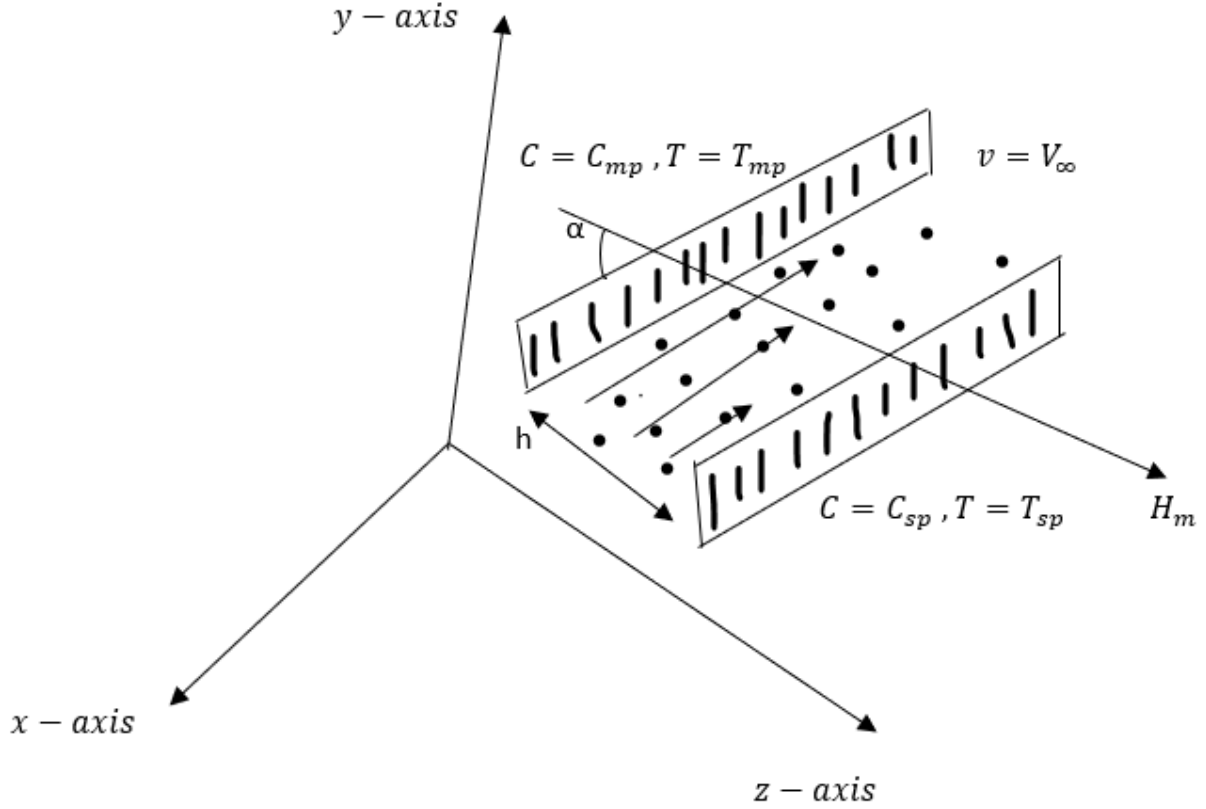

Figure 2.1: Physical Configuration of the Flow.

3   Governing equations

Assuming that the velocity of the fluid flow along the x-axis is very small compared to the velocities in y and z-axes, then $u \to 0$. Thus,

$$\frac{\partial u}{\partial x} = 0. \tag{3.1}$$

This implies that the flow variables are independent of x but only depend on y, z and time t.

3.1   Continuity equation

$$\frac{\partial v}{\partial y} + \frac{\partial w}{\partial z} = 0. \tag{3.2}$$

3.2   Navier-Stokes equation along x-axis

$$\frac{\partial u}{\partial t} + v\frac{\partial u}{\partial y} + w\frac{\partial u}{\partial z} = -\frac{\partial P}{\partial x} + \frac{\mu_\infty}{\rho_{n_f}\left(1 + \delta\left(T - T_{sp}\right)\right)}\left(\frac{\partial^2 u}{\partial y^2} + \frac{\partial^2 u}{\partial z^2}\right).$$

3.3 Navier-Stokes equation along y-axis

$$\frac{\partial v}{\partial t} + v\frac{\partial v}{\partial y} + w\frac{\partial v}{\partial z} = -\frac{\partial P}{\partial y} + \frac{\mu_\infty}{\rho_{n_f}\left(1 + \delta\left(T - T_{sp}\right)\right)}\left(\frac{\partial^2 v}{\partial y^2} + \frac{\partial^2 v}{\partial z^2}\right) + B_t g(T - T_{sp}) + B_c g(C - C_{sp}).$$

$$-\sigma\mu_e^2\left[\left(\vec{H}_m sin\alpha + \vec{H}_y\right)v - \left(\vec{H}_m cos\alpha + \vec{H}_z\right)w\right]\left(\vec{H}_m sin\alpha + \vec{H}_y\right). \tag{3.3}$$

3.4 Navier-Stokes equation along z-axis

$$\frac{\partial w}{\partial t} + v\frac{\partial w}{\partial y} + w\frac{\partial w}{\partial z} = -\frac{\partial P}{\partial z} + \frac{\mu_\infty}{\rho_{n_f}\left(1 + \delta\left(T - T_{sp}\right)\right)}\left(\frac{\partial^2 w}{\partial y^2} + \frac{\partial^2 w}{\partial z^2}\right).$$

$$+\sigma\mu_e^2\left[\left(\vec{H}_m sin\alpha + \vec{H}_y\right)v - \left(\vec{H}_m cos\alpha + \vec{H}_z\right)w\right]\left(\vec{H}_m cos\alpha + \vec{H}_z\right). \tag{3.4}$$

$$-\frac{\partial P}{\partial x} = -\frac{\partial(\rho_{n_f}gx)}{\partial x} = 0. \tag{3.5}$$

$$-\frac{\partial P}{\partial y} = -\frac{\partial(\rho_{n_f}gy)}{\partial y} = -\rho_{n_f}g. \tag{3.6}$$

$$-\frac{\partial P}{\partial y} = -\frac{\partial(\rho_{n_f}gz)}{\partial z} = 0. \tag{3.7}$$

3.5 Equation of energy

$$\frac{\partial T}{\partial t} + v\frac{\partial T}{\partial y} + w\frac{\partial T}{\partial z} = \frac{k_\infty}{\rho_{n_f}c_p}\left[1 + \epsilon\left(\frac{T - T_{sp}}{T_{mp} - T_{sp}}\right)\right]\left(\frac{\partial^2 T}{\partial y^2} + \frac{\partial^2 T}{\partial z^2}\right) +$$

$$\frac{\mu_\infty}{\rho_{n_f}c_p\left(1 + \delta(T - T_\infty)\right)}\left(4\left(\frac{\partial u}{\partial y}\right)^2 + \left(\frac{\partial v}{\partial z} + \frac{\partial w}{\partial y}\right)^2\right) + \frac{\sigma\mu_e^2\left[\left(\vec{H}_m sin\alpha + \vec{H}_y\right)v - \left(\vec{H}_m cos\alpha + \vec{H}_z\right)w\right]^2}{\rho_{n_f}c_p}. \tag{3.8}$$

3.6 Magnetic induction equation along x-axis

$$\frac{\partial\vec{H}_x}{\partial t} = 0. \tag{3.9}$$

3.7 Magnetic induction equation along y-axis

$$\frac{\partial\vec{H}_y}{\partial t} = \left(\vec{H}_m sin\alpha + \vec{H}_y\right)\frac{\partial v}{\partial z} - \left(\vec{H}_m cos\alpha + \vec{H}_z\right)\frac{\partial w}{\partial z} + v\frac{\partial\vec{H}_y}{\partial z} + \frac{1}{\mu_e\sigma}\left(\frac{\partial^2\vec{H}_z}{\partial y^2} + \frac{\partial^2\vec{H}_z}{\partial z^2}\right) \tag{3.10}$$

3.8 Magnetic induction equation along z-axis

$$\frac{\partial\vec{H}_z}{\partial t} = \left(\vec{H}_m cos\alpha + \vec{H}_z\right)\frac{\partial w}{\partial y} - \left(\vec{H}_m sin\alpha + \vec{H}_y\right)\frac{\partial v}{\partial y} - v\frac{\partial\vec{H}_y}{\partial y} + \frac{1}{\mu_e\sigma}\left(\frac{\partial^2\vec{H}_y}{\partial y^2} + \frac{\partial^2\vec{H}_y}{\partial z^2}\right). \tag{3.11}$$

3.9 Equation of concentration

$$\frac{\partial C}{\partial t} = D_m \left(\frac{\partial^2 C}{\partial y^2} + \frac{\partial^2 C}{\partial z^2} \right) - v\frac{\partial C}{\partial y} - w\frac{\partial C}{\partial z} + \frac{D_m K_t}{T_m} \left(\frac{\partial^2 T}{\partial y^2} + \frac{\partial^2 T}{\partial z^2} \right) - k_r(C - C_\infty). \qquad (3.12)$$

3.10 Initial and boundary conditions

The above equations are subject to the following initial and boundary conditions:
Initial conditions

$$t \le 0 : v = 0, w = 0, T = T_{sp}, C = C_{sp}, H_y = H_z = 0, 0 \le y, z \le h \qquad (3.13)$$

Boundary conditions

$$t > 0 : \left\{ \begin{array}{ll} v = V_\infty, w = V_\infty, T = T_{mp}, C = C_{mp}, H_y = H_z = H_m & (y, z) = 0 \\ v = 0, w = 0, T = T_{sp}, C = C_{sp}, H_y = H_y = 0 & (y, z) = h \end{array} \right\}. \qquad (3.14)$$

3.11 Non-dimensionalization process

The following non-dimensional variables have been used for the present hydromagnetic flow problem

$$H_y = H^* H_m, H_z = H_z^* H_m, y = hy^*, z = hz^*,$$

$$t = \frac{h^2 t^*}{v_{n_f}}, w = V_\infty w^*, v = V_\infty v^*, T = T_{sp} + \left(T_{mp} - T_{sp} \right) T^*, C = C_{sp} + \left(C_{mp} - C_{sp} \right) C^*, \qquad (3.15)$$

where V_∞ represents the velocity of the moving plate, (y^*, z^*) represent dimensionless cartesian coordinates, H^* represents non-dimensional induced magnetic field, C^* represents non-dimensional concentration, v_{n_f} represents kinematic viscosity, T^* represents non-dimensional temperature, v^*, w^* represent non-dimensional velocity along y and z directions respectively and h is the distance between the two plates [3].
For easy writing, let $v^* = v$, $w^* = w$, $H^* = H$, $T^* = T$, $C^* = C$, $y^* = y$ and $z^* = z$.

3.12 Continuity equation

$$\frac{\partial v}{\partial y} + \frac{\partial w}{\partial z} = 0. \qquad (3.16)$$

3.13 Navier-Stokes equation along y-axis

$$\frac{\partial v}{\partial t} + Re.v\frac{\partial v}{\partial y} + Re.w\frac{\partial v}{\partial z} = \frac{\partial^2 v}{\partial y^2} + \frac{\partial^2 v}{\partial z^2} - M.\left[\left(sin\alpha + \vec{H}_y \right) v - \left(cos\alpha + \vec{H}_z \right) w \right] \left(sin\alpha + \vec{H}_y \right). \qquad (3.17)$$

3.14 Navier-Stokes equation along z-axis

$$\frac{\partial w}{\partial t} + Re.v\frac{\partial w}{\partial y} + Re.w\frac{\partial w}{\partial z} = \frac{\partial^2 w}{\partial y^2} + \frac{\partial^2 w}{\partial z^2} + M.\left[\left(sin\alpha + \vec{H}_y \right) v - \left(cos\alpha + \vec{H}_z \right) w \right] \left(cos\alpha + \vec{H}_z \right). \qquad (3.18)$$

3.15 Equation of energy

$$\frac{\partial T}{\partial t} + Re.v\frac{\partial T}{\partial y} + Re.w\frac{\partial T}{\partial z} = \frac{1}{P_r}\left(\frac{\partial^2 T}{\partial y^2} + \frac{\partial^2 T}{\partial z^2}\right) +$$

$$E_c\left(4\left(\frac{\partial u}{\partial y}\right)^2 + \left(\frac{\partial v}{\partial z} + \frac{\partial w}{\partial y}\right)^2\right) + M.E_c\left[\left(sin\alpha + \vec{H}_y\right)v - \left(cos\alpha + \vec{H}_z\right)w\right]^2. \tag{3.19}$$

3.16 Magnetic induction equation along x-axis

$$\frac{\partial \vec{H}_x}{\partial t} = 0. \tag{3.20}$$

3.17 Magnetic induction equation along y-axis

$$\frac{\partial \vec{H}_y}{\partial t} = Re.\left(sin\alpha + \vec{H}_y\right)\frac{\partial v}{\partial z} - Re.\left(cos\alpha + \vec{H}_z\right)\frac{\partial w}{\partial z} + Re.v\frac{\partial \vec{H}_y}{\partial z} + \frac{1}{P_{r_m}}\left(\frac{\partial^2 \vec{H}_z}{\partial y^2} + \frac{\partial^2 \vec{H}_z}{\partial z^2}\right). \tag{3.21}$$

3.18 Magnetic induction equation along z-axis

$$\frac{\partial \vec{H}_z}{\partial t} = Re.\left(cos\alpha + \vec{H}_z\right)\frac{\partial w}{\partial y} - Re.\left(sin\alpha + \vec{H}_y\right)\frac{\partial v}{\partial y} - Re.v\frac{\partial \vec{H}_y}{\partial y} + \frac{1}{P_{r_m}}\left(\frac{\partial^2 \vec{H}_y}{\partial y^2} + \frac{\partial^2 \vec{H}_y}{\partial z^2}\right). \tag{3.22}$$

3.19 Equation of concentration

$$\frac{\partial C}{\partial t} = \frac{1}{S_c}\left(\frac{\partial^2 C}{\partial y^2} + \frac{\partial^2 C}{\partial z^2}\right) - Re.v\frac{\partial C}{\partial y} - Re.w\frac{\partial C}{\partial z} + S_r\left(\frac{\partial^2 T}{\partial y^2} + \frac{\partial^2 T}{\partial z^2}\right) - \gamma C. \tag{3.23}$$

3.20 Non-dimensional initial and boundary conditions

The above equations are subject to the following initial and boundary conditions:
Initial conditions

$$t \leq 0 : v = 0, w = 0, T = 0, C = 0, H_y = H_z = 0, 0 \leq (y,z) \leq 1 \tag{3.24}$$

Boundary conditions

$$t > 0 : \begin{cases} w = 1, v = 1, T = 1, C = 1, H_y = H_z = 1 & (y,z) = 0 \\ v = 0, w = 0, T = 0, C = 0, H_y = H_y = 0 & (y,z) = 1 \end{cases}. \tag{3.25}$$

4 Finite difference form of the governing equations

The finite difference method has been employed to approximate the nonlinear partial differential equations as algebraic difference expressions, which were then simulated in MATLAB. The step sizes for the spatial coordinates and time are set to $\Delta t = 0.00001$ and $\Delta y = \Delta z = 0.02$ respectively.

4.1   Navier-Stokes equation along y-axis

$$v_j^{k+1} = v_j^k - Re.v.\Delta t \frac{v_{j+1}^k - v_{j-1}^k}{2\Delta y} - Re.w.\Delta t \frac{v_{j+1}^k - v_{j-1}^k}{2\Delta z} + \frac{v_{j+1}^k - 2v_j^k + v_{j-1}^k}{(\Delta y)^2} +$$

$$\frac{v_{j+1}^k - 2v_j^k + v_{j-1}^k}{(\Delta z)^2} - M. \left[\left(sin\alpha + \vec{H}_{y_j}^k \right) v_j^k - \left(cos\alpha + \vec{H}_{z_j}^k \right) w_j^k \right] \left(sin\alpha + \vec{H}_{y_j}^k \right). \tag{4.1}$$

4.2   Navier-Stokes equation along z-axis

$$w_j^{k+1} = w_j^k - Re.v.\Delta t \frac{w_{j+1}^k - w_{j-1}^k}{2\Delta y} - Re.w.\Delta t \frac{w_{j+1}^k - w_{j-1}^k}{2\Delta z} + \frac{w_{j+1}^k - 2w_j^k + w_{j-1}^k}{(\Delta y)^2} +$$

$$\frac{w_{j+1}^k - 2w_j^k + w_{j-1}^k}{(\Delta z)^2} - M. \left[\left(sin\alpha + \vec{H}_{y_j}^k \right) v_j^k - \left(cos\alpha + \vec{H}_{z_j}^k \right) w_j^k \right] \left(cos\alpha + \vec{H}_{z_j}^k \right). \tag{4.2}$$

4.3   Equation of energy

$$T_j^{k+1} = T_j^k - Re.v_j^k \Delta t \left(\frac{T_{j+1}^k - T_{j-1}^k}{2\Delta y} \right) - Re.w_j^k \Delta t \left(\frac{T_{j+1}^k - T_{j-1}^k}{2\Delta z} \right) + \frac{1}{P_r}.\Delta t \left(\frac{T_{j+1}^k - 2T_j^k + T_{j-1}^k}{(\Delta y)^2} \right) +$$

$$\frac{1}{P_r}.\Delta t \left(\frac{T_{j+1}^k - 2T_j^k + T_{j-1}^k}{(\Delta z)^2} \right) + E_c.\Delta t \left(4 \left(\frac{u_{j+1}^k - u_{j-1}^k}{2\Delta y} \right)^2 + \left(\frac{u_{j+1}^k - u_{j-1}^k}{2\Delta z} + \frac{w_{j+1}^k - w_{j-1}^k}{2\Delta y} \right)^2 \right) +$$

$$\tag{4.3}$$

$$M.E_c.\Delta t \left[\left(sin\alpha + \vec{H}_{y_j}^k \right) v_j^k - \left(cos\alpha + \vec{H}_{z_j}^k \right) w_j^k \right]^2. \tag{4.4}$$

4.4   Magnetic induction equation along x-axis

$$\frac{\vec{H}_{x_j}^{k+1} - \vec{H}_{x_j}^k}{\Delta t} = 0. \tag{4.5}$$

4.5   Magnetic induction equation along y-axis

$$\vec{H}_{y_j}^{k+1} = \vec{H}_{y_j}^k + Re.\Delta t \left(sin\alpha + \vec{H}_{y_j}^{\,k} \right) \left(\frac{v_{j+1}^k - v_{j-1}^k}{\Delta z} \right) + Re.v_j^k \Delta t \left(\frac{\vec{H}_{y_{j+1}}^{\,k} - \vec{H}_{y_{j-1}}^{\,k}}{\Delta z} \right).$$

$$-Re.\Delta t \left(cos\alpha + \vec{H}_{z_j}^{\,k} \right) \left(\frac{w_{j+1}^k - w_{j-1}^k}{\Delta z} \right) + \frac{\Delta t}{P_{r_m}} \left(\frac{\vec{H}_{z_{j+1}}^{\,k} - 2\vec{H}_{z_j}^{\,k} + \vec{H}_{z_{j-1}}^{\,k}}{(\Delta y)^2} + \frac{\vec{H}_{z_{j+1}}^{\,k} - 2\vec{H}_{z_j}^{\,k} + \vec{H}_{z_{j-1}}^{\,k}}{(\Delta z)^2} \right).$$

$$\tag{4.6}$$

4.6 Magnetic induction equation along z-axis

$$\vec{H}_{y_j}^{k+1} = \vec{H}_{y_j}^k + Re.\Delta t \left(cos\alpha + \vec{H}_{z_j}^{\ k}\right) \left(\frac{w_{j+1}^k - w_{j-1}^k}{\Delta y}\right) + Re.v_j^k\Delta t \left(\frac{\vec{H}_{y_{j+1}}^{\ k} - \vec{H}_{y_{j-1}}^{\ k}}{\Delta y}\right)$$

$$-Re.\Delta t \left(sin\alpha + \vec{H}_{y_j}^{\ k}\right) \left(\frac{v_{j+1}^k - v_{j-1}^k}{\Delta y}\right) + \frac{\Delta t}{Pr_m} \left(\frac{\vec{H}_{y_{j+1}}^{\ k} - 2\vec{H}_{y_j}^{\ k} + \vec{H}_{y_{j-1}}^{\ k}}{(\Delta y)^2} + \frac{\vec{H}_{y_{j+1}}^{\ k} - 2\vec{H}_{y_j}^{\ k} + \vec{H}_{y_{j-1}}^{\ k}}{(\Delta z)^2}\right).$$

$$(4.7)$$

4.7 Equation of concentration

$$C_j^{k+1} = C_j^k + \frac{\Delta t}{S_c} \left(\frac{C_{j+1}^k - 2C_j^k + C_{j-1}^k}{(\Delta y)^2} + \frac{C_{j+1}^k - 2C_j^k + C_{j-1}^k}{(\Delta z)^2}\right) - Re.v_j^k.\Delta t \left(\frac{C_{j+1}^k - C_{j-1}^k}{2\Delta y}\right) -$$

$$Re.w_j^k.\Delta t \left(\frac{C_{j+1}^k - C_{j-1}^k}{2\Delta z}\right) + S_r.\Delta t \left(\frac{T_{j+1}^k - 2T_j^k + T_{j-1}^k}{(\Delta y)^2} + \frac{T_{j+1}^k - 2T_j^k + T_{j-1}^k}{(\Delta z)^2}\right) - \gamma C^*.\Delta t. \quad (4.8)$$

4.7.1 Initial and boundary conditions in finite difference form

From equations 26 to 33 the corresponding initial and boundary conditions in non-dimensional form are:
Initial conditions

$$t \leq 0 : v(j,0) = 0, w = 0, T(j,0) = 0, C(j,0) = 0, H_y(j,0) = H_z(j,0) = 0, 0 \leq (y,z) \leq 1. \quad (4.9)$$

Boundary conditions

$$t > 0 : \left\{\begin{array}{ll} v(0,k) = 1, w(0,k) = 1, T(0,k) = 1, C(0,k) = 1, H_y(0,k) = H_z(0,k) = 1 & (y,z) = 0 \\ v(j,k) = 0, w(j,k) = 0, T(j,k) = 0, C(j,k) = 0, H_y(j,k) = H_z(j,k) = 0 & (y,z) = 1 \end{array}\right\}.$$

$$(4.10)$$

5 Results and discussion

Figures 2 and 3 demonstrate that as the angle of inclination of the applied magnetic field increases, the fluid velocity decreases. This is because a larger inclination angle strengthens the applied magnetic field, thereby increasing the Lorentz force. The enhanced Lorentz force acts against the fluid flow, resulting in a reduction in the fluid's velocity within the flow problem.

Figures 4 and 5 show that an increase in the Reynolds number (Re) leads to an increase in the velocity profiles. [3] The Reynolds number measures the balance between inertial forces and viscous forces in fluid flow. A higher Reynolds number suggests weaker viscous forces, enabling fluid particles to move more rapidly due to reduced resistance. On the other hand, a lower Reynolds number indicates stronger viscous forces, leading to greater resistance and, consequently, a slower fluid velocity. Figure 6 shows that increasing the Prandtl number leads to a decrease in the temperature of the fluid. [6] The Prandtl number plays a critical role in determining the heat transfer behavior of a fluid, as it affects the mechanisms of heat transfer
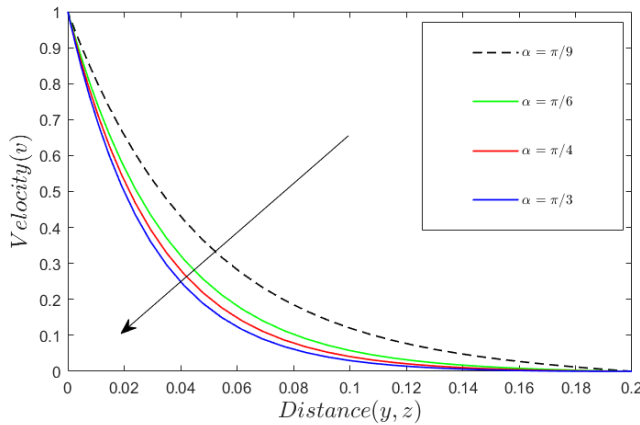
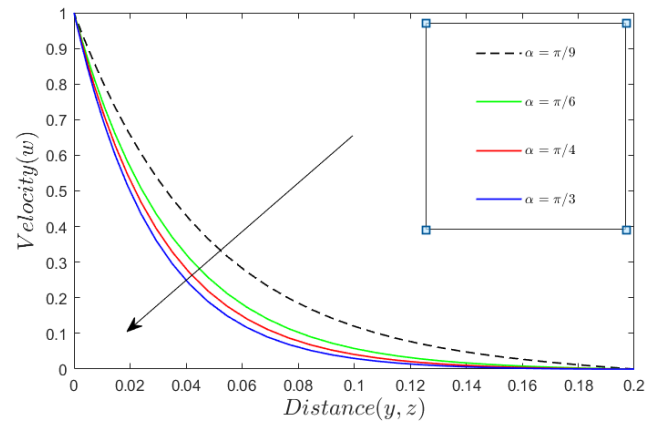Figure 5.1: Velocity profiles (v) for different values of α.

Figure 5.2: Velocity profiles (w) for different values of α.
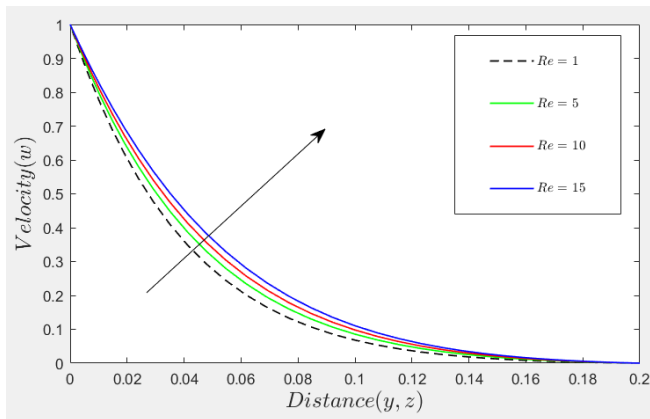

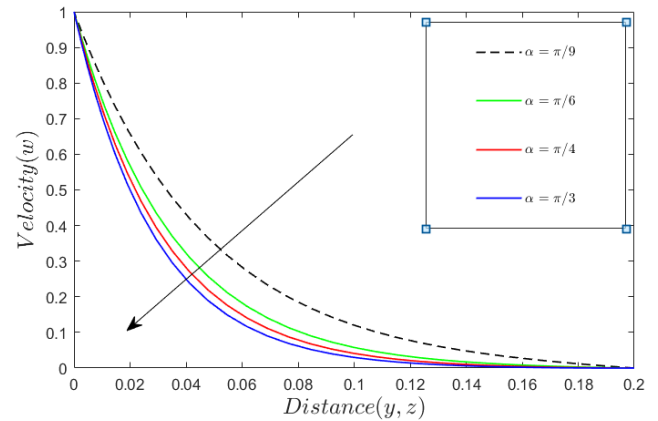Figure 5.3: Velocity profiles (w) for different values of Re.

Figure 5.4: Velocity profiles (v) for different values of Re.

within the fluid and to surrounding surfaces. Observations indicate that as the Prandtl number increases, the fluid temperature decreases. Defined as the ratio of momentum diffusivity to thermal diffusivity, a higher Prandtl number implies reduced thermal diffusivity and increased viscosity. This reduction in thermal diffusivity leads to a thinner thermal boundary layer, resulting in lower fluid temperatures. Figure 7 illustrates that the temperature of the nanofluid rises with an increase in the Eckert number. The Eckert number, defined as the ratio of the flow's kinetic energy to its enthalpy, highlights that higher values signify a dominance of kinetic energy over enthalpy. This dominance promotes convective heating, where the kinetic energy of the fluid is transformed into thermal energy as it moves over a stretching plate. This process generates internal energy, leading to a rise in the fluid's temperature [7]. Figure 8 illustrates that fluid temperature increases with a higher magnetic number. The magnetic number, representing the ratio of magnetic forces to fluid inertia forces, indicates that stronger magnetic forces and weaker inertia forces correspond to higher values. As moving fluid particles interact with an intensified magnetic field, and an electric current is generated. Collisions between fluid particles and the charged particles from this current induce vibrations, which produce heat in the form of thermal energy. Thus, a rise in the magnetic number
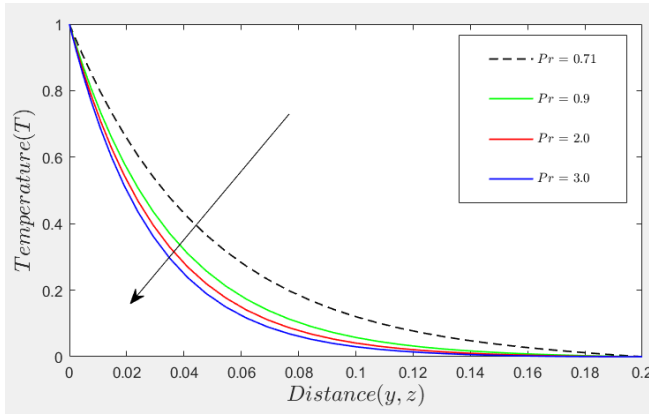
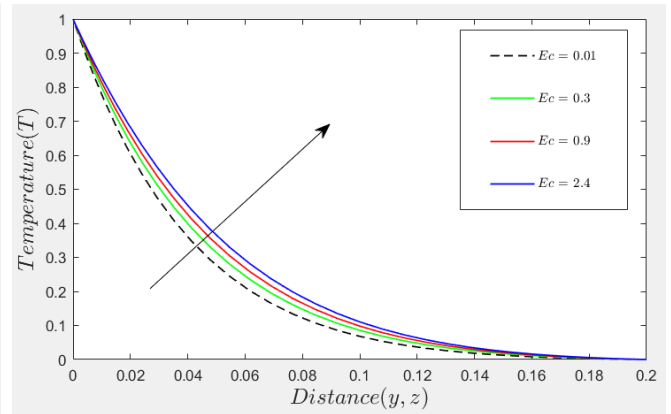Figure 5.5: Temperature profiles (T) for different values of P_r.

Figure 5.6: Temperature profiles (T) for different values of Ec

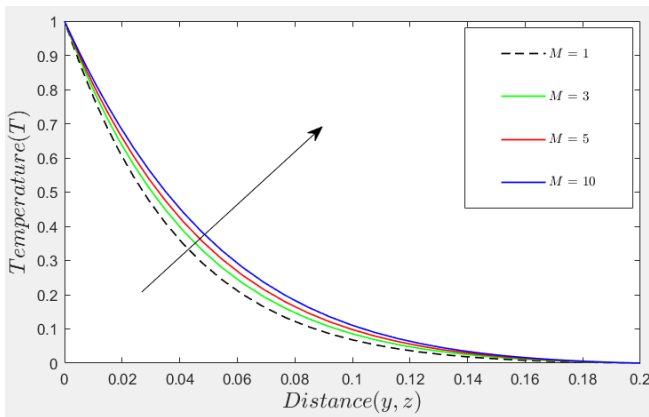leads to an increase in the fluid's temperature [6]. Figure 9 shows that increasing the Reynolds

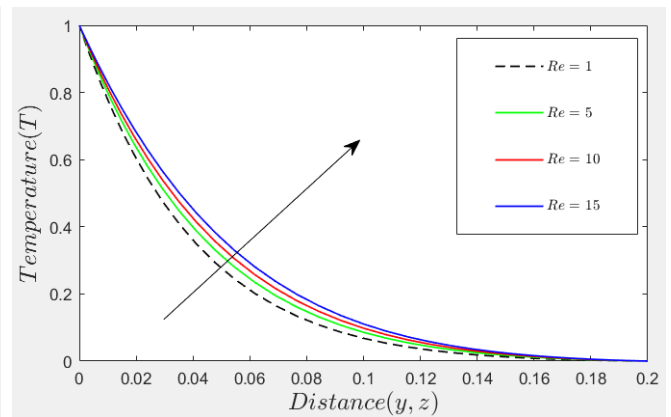Figure 5.7: Temperature profiles (T) for different values of M.

Figure 5.8: Temperature profiles (T) for different values of Re.

number leads to an increase in the temperature profiles. Since Reynolds number is the ratio of inertia forces to viscous forces, so increasing the Reynolds number implies that the viscous forces become less significant. A decrease in viscous forces means that fluid particles have increased motion and heat is generated due to the collision of the particles which are moving at high velocity thereby increasing fluid temperature

Figures 10 and 13 show that increasing magnetic Prandtl number leads to a decrease in induced magnetic field long y and z directions. Since the magnetic Prandtl number is the ratio of momentum diffusivity to the magnetic diffusivity, so increasing the magnetic Prandtl number implies a reduction in magnetic diffusivity, which leads to a decrease in the induced magnetic field by the motion of the conducting medium and thus induced magnetic profiles along y and z decrease. Figures 11 and 12 show that an increase in the Reynolds number leads to an increase in the induced magnetic field profiles along the y and z directions. The Reynolds number, being the ratio of inertial forces to viscous forces, implies that a higher Reynolds number corresponds to reduced viscous forces. This reduction in viscous forces enhances the interaction between the fluid and the magnetic field, thereby increasing the induced magnetic field in both the y and z directions [17]. Figure 14 shows that the concentration of the
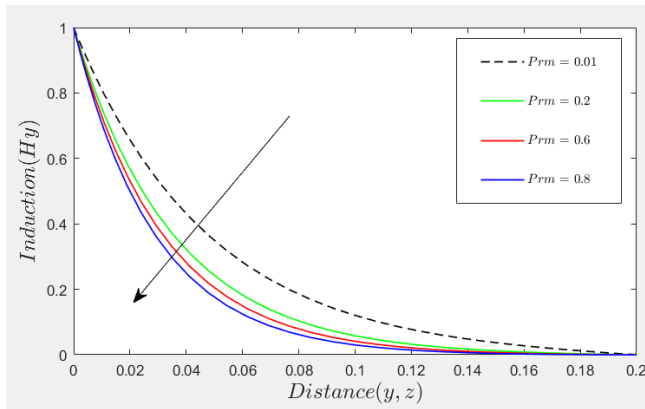
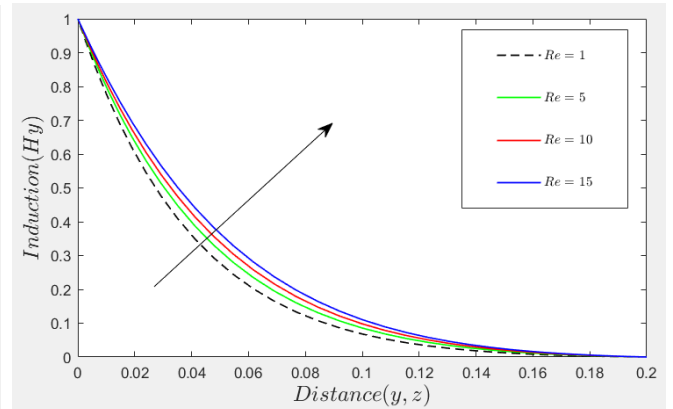Figure 5.9: Magnetic induction profiles along y (Hy) for different values of P_{r_m}.

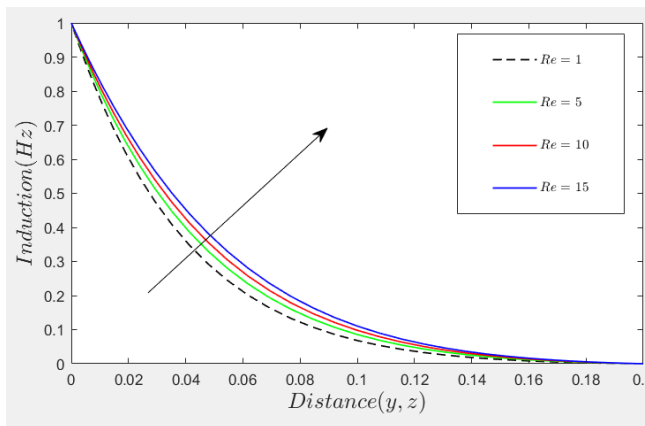Figure 5.10: Magnetic induction profiles along y (Hy) for different values of *Re*.

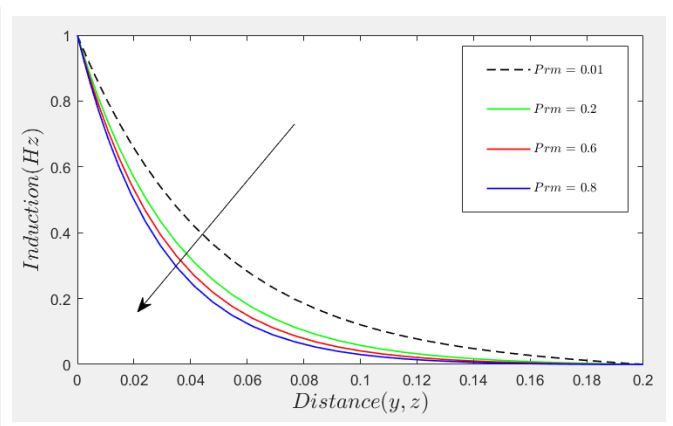Figure 5.11: Magnetic induction profiles along z (Hz) for different values of *Re*.

Figure 5.12: Magnetic Induction profiles along z (Hz) for different values of P_{r_m}.

nanofluid decreases as the Schmidt number increases. The Schmidt number, being the ratio of momentum diffusivity to mass diffusivity of particles, indicates that a higher Schmidt number corresponds to reduced mass diffusivity. This reduction in mass diffusivity results in a decrease in the concentration profiles of the nanofluid. Figure 15 shows that an increase in the chemical reaction parameter leads to a decrease in the concentration of the fluid particles [11]. A higher chemical reaction parameter indicates that the chemical reaction proceeds at a faster rate relative to fluid transport. As a result, more reactants are consumed or converted into products in a given time, leading to a decrease in the concentration of the reactants in the fluid. In a chemical reaction, the concentration of reactant species decreases as they undergo chemical changes to form products. As the reaction progresses, reactant molecules collide and react, forming new products. Consequently, the concentration of the reacting species decreases because the molecules are being converted into products, leading to a decrease in chemical molecular diffusivity [10].

Figure 16 shows that increasing the Soret number increases concentration profiles [10]. The Soret number determines the effect of temperature gradients on inducing significant mass diffusion effects. Increasing the Soret number generates a mass flux that leads to an increase in the mass boundary layer thickness, thereby increasing the concentration of the fluid.
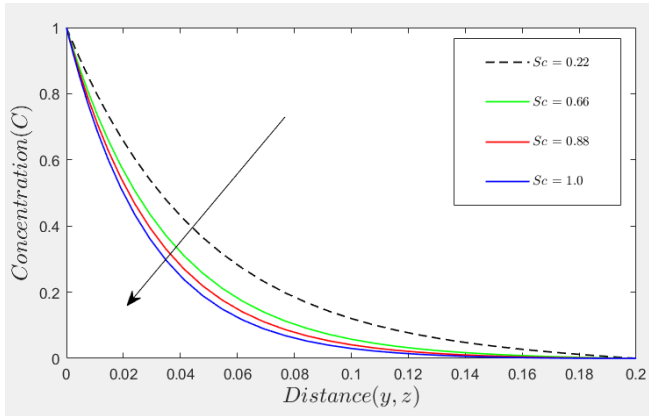
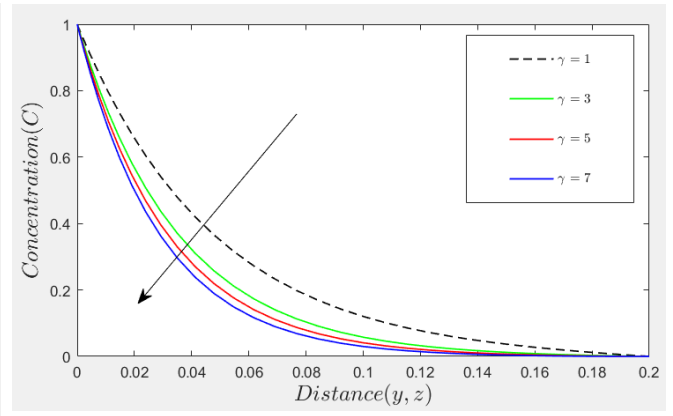Figure 5.13: Concentration profiles (C) for different values of Sc.

Figure 5.14: Concentration profiles (C) for different values of γ.

In Figure 17, it is shown that increasing the magnetic number leads to a decrease in the velocity profile. This is because a higher magnetic number enhances the Lorentz force, which resists the fluid flow and thus reduces the velocity of the fluid. [3, 6].
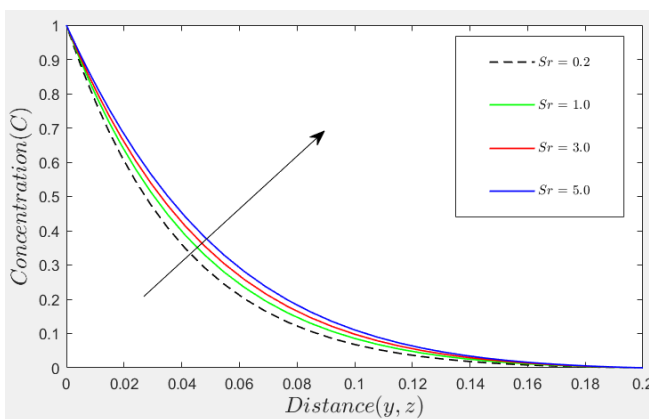

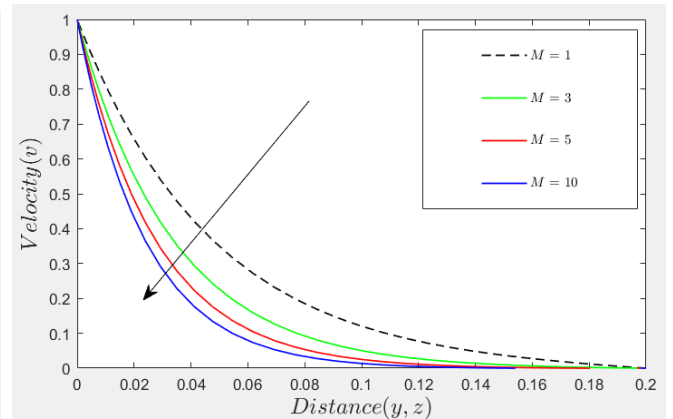Figure 5.15: Concentration profiles (C) for different values of Sr.

Figure 5.16: Velocity profiles (v) for different values of M.

Conclusion

Von-Neumann stability analysis was conducted to check the stability and convergence of the mathematical model developed. From the results, it is observed that increasing values of Reynolds number leads to an increase in velocity profiles while increasing values of magnetic number and angle of inclination leads to a decrease in the velocity profile. Increasing values of Reynolds number, Eckert number, magnetic parameter leads to increase in temperature profile while increasing the values of the Prandtl number leads to a decrease in temperature profile. Increasing values of Reynolds number leads to an increase in induced magnetic field profiles while increasing values of magnetic Prandtl number leads to a decrease in induced magnetic field profiles. Increasing the values of the Soret number leads to an increase in concentration profiles while increasing values of Schmidt number and chemical reaction parameter leads to a decrease in concentration profile.

Data availability

Conflicts of interest

Funding statement

Acknowledgment

References

[1] H. A. Attia, and N. A. Kotb, *MHD flow between two parallel plates with heat transfer*, Acta mechanica, **117**(1) (1996), 215–220. DOI

[2] Y. M. Chu, S. Bashir, M. Ramzan, and M. Y. Malik, *Modelbased comparative study of magnetohydrodynamics unsteady hybrid nanofluid flow between two infinite parallel plates with particle shape effects*, Mathematical Methods in the Applied Sciences, **46**(10) (2023), 11568–11582. DOI

[3] M. Danny, T. Kafunda, K. Christian, and J. Stanley, *Analysis on Heat and Mass Transfer in Boundary Layer Non-Newtonian Nanofluid Flow Past a Vertically Stretching Porous Plate with Chemical Reaction, Variable Magnetic Field and Variable Thermal Conductivity*, International Journal of Advanced Applied Mathematics and Mechanics, **11**(4) (2024), 1–14.

[4] A. S. Dogonchi, M. Waqas, S. R. Afshar, S. M. Seyyedi, M. Hashemi-Tilehnoee, A. J. Chamkha, and D. D. Ganji, *Investigation of magneto-hydrodynamic fluid squeezed between two parallel disks by considering Joule heating, thermal radiation, and adding different nanoparticles*, International Journal of Numerical Methods for Heat and Fluid Flow, **30**(2) (2020), 659–680. DOI

[5] M. D. Ikram, M. I. Asjad, A. Akgül, and D. Baleanu, *Effects of hybrid nanofluid on novel fractional model of heat transfer flow between two parallel plates*, Alexandria Engineering Journal, **60**(4) (2021), 3593–3604. DOI

[6] T. Kafunda, M. Danny, K. Christian, J. Stanley, and E. Ambe, *Unsteady hydromagnetic non-Newtonian nanofluid flow past a porous stretching sheet in the presence of variable magnetic field and chemical reaction*, Journal of Applied Mathematics and Physics, **11**(9) (2023), 2545–2567. DOI

[7] D. Kumar, A. Singh, and D. Kumar, *Effect of Hall current on the magnetohydrodynamic free convective flow between vertical walls with induced magnetic field*, The European Physical Journal Plus, **133**(5) (2018), 207. DOI

[8] L. Lugo, J. P. Vallejo, G. Zyla, and J. Fernandez-Seara, *Rheological behaviour of functionalized graphene nanoplatelet nanofluids based on water and propylene glycol: water mixtures*, International Communications in Heat and Mass Transfer, **99** (2018), 43–53. DOI

[9] R. Mohebbi, S. Mehryan, M. Izadi, and O. Mahian, *Natural convection of hybrid nanofluids inside a partitioned porous cavity for application in solar power plants*, Journal of Thermal Analysis and Calorimetry, **137** (2019), 1719–1733. DOI

[10] N. Mwamba, J. Okelo Abonyo, K. O. Awuor, B. Otieno, A. Lwande, and J. O. Owino, *Effects of thermal radiation and chemical reaction on hydromagnetic fluid flow in a cylindrical collapsible tube with an obstacle*, International Journal of Mathematics and Mathematical Sciences, (2023). DOI

[11] M. Ramzan, S. Inam, and S. Shehzad, *Three-dimensional boundary layer flow of a viscoelastic nanofluid with Soret and Dufour effects*, Alexandria Engineering Journal, **55**(1) (2016), 311–319. DOI

[12] A. M. Rashad, A. J. Chamkha, M. Ismael, and T. Salah, *MHD Natural Convection in a Triangular Cavity filled with a CuAl2O3/Water Hybrid Nanofluid with Localized Heating from Below and Internal Heat Generation*, Journal of Heat Transfer, **7 140**(7) (2018), 072502. DOI

[13] S. A. R. Sahebi, H. Pourziaei, A. R. Feizi, M. H. Taheri, Y. Rostamiyan, and D. D. Ganji, *Numerical analysis of natural convection for non-Newtonian fluid conveying nanoparticles between two vertical parallel plates*, The European Physical Journal Plus, **130** (2015), 1–12. DOI

[14] S. Salehi, A. Nori, K. Hosseinzadeh, and D. D. Ganji, *Hydrothermal analysis of MHD squeezing mixture fluid suspended by hybrid nanoparticles between two parallel plates*, Case Studies in Thermal Engineering, **21** (2020), 100650. DOI

[15] A. Shahsavar, M. Moradi, and M. Bahiraei, *Heat transfer and entropy generation optimization for flow of a non-Newtonian hybrid nanofluid containing coated CNT/Fe3O4 nanoparticles in a concentric annulus*, Journal of the Taiwan Institute of Chemical Engineers, **84** (2018), 28–40. DOI

[16] J. P. Vallejo, L. Lugo, G. Zyla, and J. Fernandez-Seara, *Influence of Six Carbon-Based Nanomaterials on the Rheological Properties of Nanofluids*, Nanomaterials, **9**(2) (2019), 146. DOI

[17] A. S. Yadav, R. K. Khare, and M. James, *Fluid flow through porous medium in a horizontal channel in inclined magnetic field*, Journal of Applied Science and Computations, **6**(1) (2019), 1223–1226.

Appendix

Nomenclature

Symbol	Meaning
P	Pressure (Nm^{-2})
T	Temperature (K)
C	Species concentration ($mole/Kg$)
T_{mp}	Temperature of the nanofluid on the moving plate (K)
T_{sp}	Temperature of the nanofluid on the stationary plate (K)
c_p	Specific heat capacity at constant pressure ($JKg^{-1}k^{-1}$)
C_{mp}	Concentration of the nanofluid at the moving plate ($mole/Kg$)
C_{sp}	Concentration of the nanofluid at the stationary plate ($mole/Kg$)
D_m	Mass diffusivity/Chemical molecular diffusivity (m^2s^{-1})
$\vec{H}_m$	Applied magnetic field (Wbm^{-2})
k_{n_f}	Coefficient of the thermal conductivity of the nanofluid ($Wm^{-1}k^{-1}$)
t	Time (s)
$\vec{H}_x$	Induced magnetic field along x direction (Am^{-1})
$\vec{H}_y$	Induced magnetic field along y direction (Am^{-1})
$\vec{J}$	Current density (Am^{-2})
$\vec{H}$	Magnetic field strength (Am^{-1})
T_m	Mean fluid temperature (K)
K_t	Thermal diffusion ratio (m^2s)
k_p	Darcy permeability (m^2)
k_r	Chemical reaction coefficient
Re	Reynolds number
Pr	Prandtl number
Pr_m	Magnetic Prandtl number
Sr	Soret number
Sc	Schmidt number
M	Magnetic number
γ	Chemical reaction parameter
Ec	Eckert number
α	Angle of inclination
μ_{n_f}	Coefficient of dynamic viscosity of the nanofluid $Kgm^{-1}s^{-1}$
ρ_{n_f}	Density of the nanofluid (Kgm^{-3})
σ	Electrical conductivity (Sm^{-1})
μ_e	Magnetic permeability (Hm^{-1})
ν_{n_f}	Kinematic viscosity of the nanofluid (m^2s^{-1})